NOISE SOURCE LOCALISATION IN A LOW SPEED AUTOMOTIVE ENGINE COOLING MODULE

Yann PASCO, Gyuzel YAKHINA, Stéphane MOREAU

Université de Sherbrooke, 2500 boulevard de l'Université, Sherbrooke, QC, J1K1R1, Canada

ABSTRACT

Noise sources in a typical automotive engine cooling module have been studied at several operating conditions obtained by varying both the rotational speed and the volume flow rate. Directivity measurements and microphone-array source localization have been combined to first verify the proper dipolar scaling of the sound emitted by the module, and then to localize the noise sources beyond 4 kHz at the tip blade leading edge stressing that, for this particular engine cooling module, the turbulence-interaction noise generated by the secondary flow in the tip region appears to be the dominant broadband noise mechanism at all the frequencies resolved by the ROSI beamforming algorithm. For the first time, the latter technique is also shown to work fine in the presence of the heat exchanger between the antenna and the fan, which does not prevent the correct reconstruction of the sound sources.

INTRODUCTION

The sound generated by rotating machines is a topic that is becoming more and more relevant. In fact, this noise is an environmental concern in many industrial fields ranging from energy production to transportation systems or daily appliances [1-2]. The rotating machine studied here is an automotive engine cooling fan system. The noise produced by these fans is a major contributor to the total radiated noise in a car, and in certain cases it can dominate over other sources like the engine or the tires (rolling noise). Usually, the fan is extracting air through a heat exchanger where a coolant fluid is circulating through a network of tubing. The heat exchanger is usually located close to the fan on its suction side. This creates a turbulent flow and participates to the generation of broadband noise [3]. As the module is located in the engine bay, the upstream flow is distorted and the engine creates a blockage downstream, which leads to a strong tonal noise contribution. The impact of those distortions on the blades or struts generates tonal noise.

The article aims at evaluating the contribution of acoustic sources located on the rotor blades. The source localization for rotating machine should take into account the Doppler effect as the sources are rotating with the fan. Classical beamforming works but it leads to continuous annulus sources.

Sitjsma *et al.* [4] propose to solve this problem by using a transfer function for a moving monopole source in uniform flow to reconstruct the signal in the time domain and develop an algorithm able to deal with rotating sources, named ROtating Source Identifier (ROSI). Using this method, the measurement of the sound pressure of rotating sources can be done using an array of microphones. The proper implementation of the method was verified using the benchmark from [5]. In the present study, a 60-microphones logarithmic array was used and the reconstruction of sound pressure level was done in third octave bands. Measurements were done at different rotational speeds of the fan in the anechoic wind tunnel at Université de Sherbrooke (UdeS), without any other flow restriction than the heat exchanger itself. Measurements were also done at full RPM with and without heat exchanger to compare if it is transparent acoustically, and verify if noise sources can be properly detected within a module behind a heat exchanger stack. Directivity measurements were conducted as well. Both methods have been compared on the central microphone of the microphone array. Note that the present study is part of a collaborative project between UdeS and the Von Karman Institute (VKI), the major aim of which is to conduct a comparative experimental investigation of fan noise in two different facilities to yield a reference database on such automotive engine cooling modules [6].

EXPERIMENTAL BACKGROUND

Configuration description

The investigated automotive engine cooling module has an axial fan of diameter D = 380 mm shown in Figure 1. It has 7 blades made of bulbous airfoils. The blades are bi-swept with a high forward sweep at the tip. This fan has been designed for the following operating conditions: a flow rate of 2100 m³/h, a total-to-static pressure difference Δp of 180 Pa, at 3400 rpm.

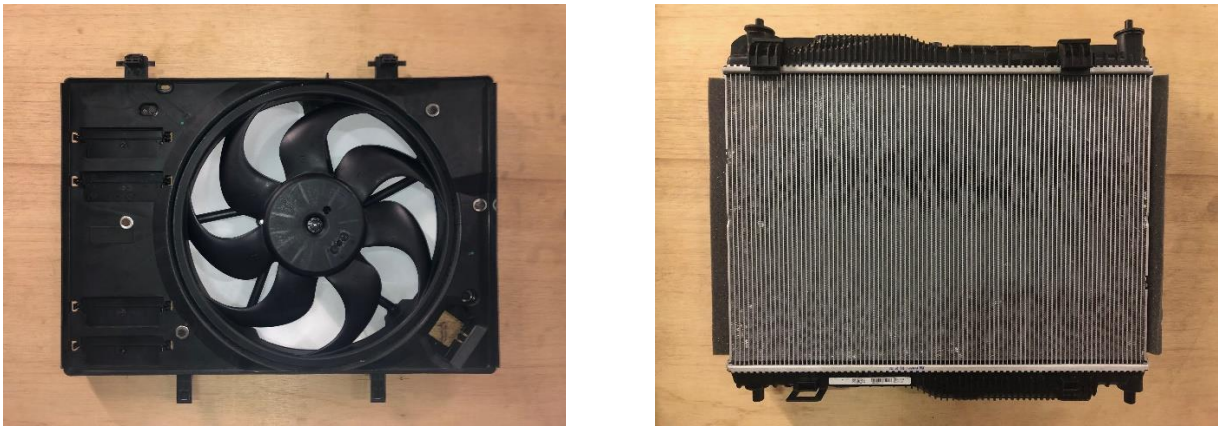

Figure 1: Automotive engine cooling module; left: fan system and shroud; right: heat exchanger.

The performance curves of the module are shown in *Figure 2*. Note that FA corresponds to the Fan alone, FM to the full module and OP the several tested operating conditions tested at VKI. Three other rotational speeds have been tested at UdeS and reported here: 1500, 2000 and 2400 rpm. Two configurations have also been investigated: one without the heat exchanger shown in Figure 1 (left) and the other with the heat exchanger shown in *Figure 1* (right). The former case refers to free flow conditions (Δp = 0 Pa, very close to the 1 kg/s operating point shown in the FM characteristics in Figure 2). The latter case stands for the intersection between the heat exchanger resistance (black dashed-dotted line) and the FM curve (red dashed line). For the above operating conditions, the blade-passing frequency (BPF) is 397 Hz.

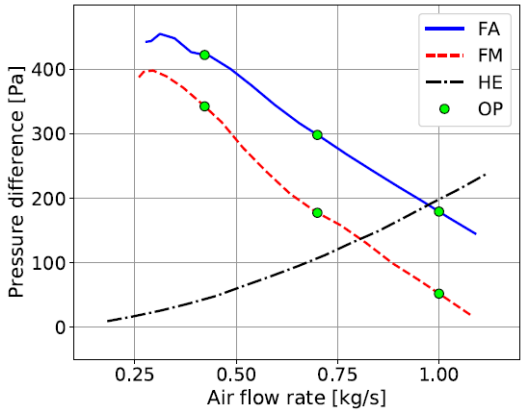

Figure 2: Performance curves at nominal 3400 rpm: pressure rise vs volume flow rate.

Acoustic measurements

Acoustic directivity and source-localization measurements have been conducted on the engine cooling module shown in Figure 1 in the anechoic open-jet wind tunnel at UdeS. The latter has a low cut-off frequency of 100 Hz and a very low background noise (below -20 dB) and turbulence intensity (about 0.4 %), which can then properly capture spectra for all rotational speeds up to the 10-20 kHz, over the whole frequency range of interest. This was previously demonstrated on a smoke-removal fan system used by firemen [7-8]. As shown in Figure 3, the sound pressure levels have been measured in free field with thirteen 1/4 inch free-field Brüel & Kjær microphones, placed in a semicircle at a radius of 1.8 m around the module centered on the fan rotational axis in a vertical plane centered on the fan rotational axis. Note this is the same arc as used in the previous study on the smoke-removal fan system, but hanged from the ceiling instead of being placed in a horizontal plane. Windscreens are employed on the downstream microphones (12 and 13) to mitigate the influence of the flow. In Figure 2, the flow comes from right to left (air is pulled through the heat exchanger) and we see the back of the fan system and the shroud. The module is clamped by the heat exchanger water tanks on two solid posts that hold the module vertical about 1 m above the ground. For all microphones, the pressure signals are recorded for 30 s with a sampling frequency of 65.536 kHz.

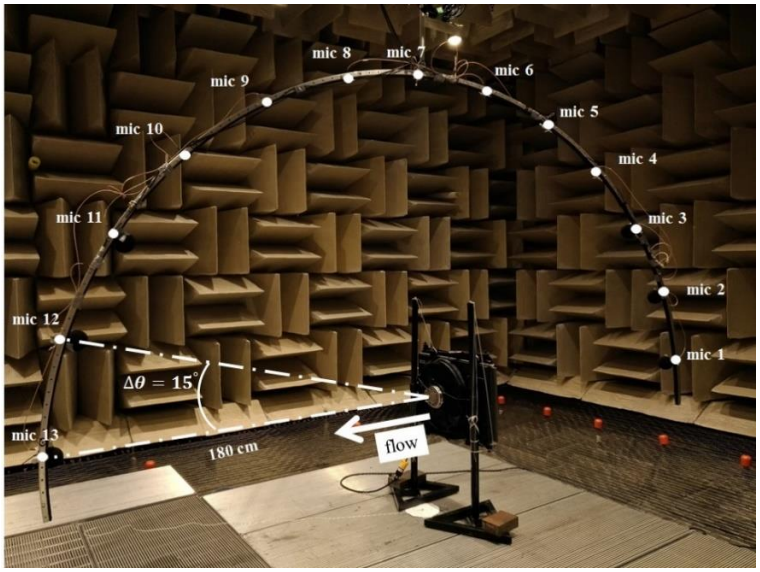

Figure 3: Directivity measurements at UdeS.

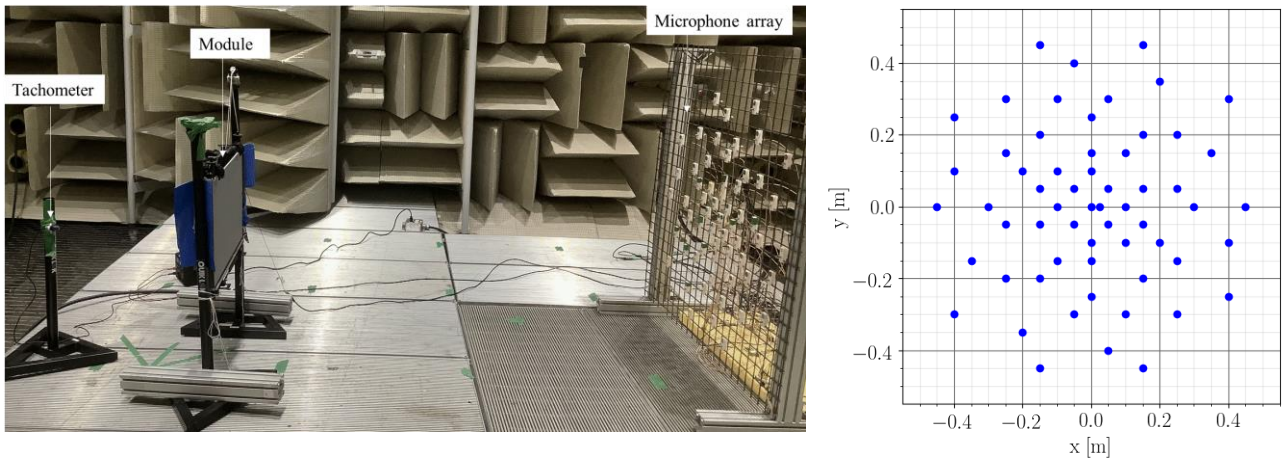

Figure 4: Source localizarion set-up at UdeS (left) and microphone arrangement (right)

The corresponding source-localization set-up is presented in Figure 4 (left). The same assembly as in the directivity measurement is made to hold the module. A tachometer is placed in front of the fan systems to track the fan rotational speed. The microphone array with 60 microphones (Brüel & Kjær) is placed on the other side facing the heat exchanger. The microphone array has a diameter D_a = 0.9 m and is designed with the spiral arrangement shown in Figure 4 (right). Two different distances were considered between the module and the microphone array (right): 2 m (as in Figure 4) and 0.95 m (2.5 D), the results of which are reported below. All signals are again recorded for 30 s with a sampling frequency of 65.536 kHz. The minimum resolvable source separation R at a given frequency f is then given by the Rayleigh criterion (c_0, speed of sound):

$$R \approx 2.5\, D \tan\left(\frac{1.22\, c_0}{f D_a}\right)$$

RESULTS

Directivity measurements

The spectra obtained at various rotational speeds (rpm) on microphone 1 (on the rotational axis in front of the module) are presented in Figure 5. All spectra have similar shape with similar tonal and broadband contributions [9-10]. Similar results are obtained on the other microphones. At the nominal speed of 3400 rpm, three main tones are seen. The first tone at about 280 Hz corresponds to 5 rev (harmonic of the rotational frequency), and is caused by unbalance induced vibration. The other two at about 400 and 800 Hz correspond to the first and second BPF. For all rotational speeds the broadband component has similar shape: an almost flat, constant level spectrum up to 1 kHz; similar humps and peaks at high frequencies that remain at the same frequencies independently of the variation of rotational speed. Beyond the roll-off at 4 kHz, the features of the spectra, particularly the sharp trough at 7 kHz, have corresponding acoustic wavelengths that are comparable with the dimensions of the shroud and other components of the module or the assembly (posts). Therefore, this part of the spectra is most likely influenced by the experimental setup, and is very similar to what was observed on the smoke-removal fan system at high frequencies (see trough at 6 kHz in *Figure 5* in [8]). The same separation of noise sources and calculation of the transfer path as used in [7-8] would most likely remove this installation artefact as was shown in Figure 6 in [7] for instance. Recent measurements on the same module in the VKI ALCOVES anechoic wind tunnel also confirm the spectral shape up to the roll-off, but have a smoother decay at high

frequencies, suggesting again installation effect at high frequencies [6]. Moreover, in both test facilities, similar spectral shapes are observed with and without the heat exchanger (see Figure 8 in [6]), which is consistent with what was observed by Rynell *et al.* [11] on a similar engine cooling module with the same technology but for trucks. Note that a different trend was observed by Czwielong *et al.* [12], but with a different heat exchanger technology and module architecture, which yielded larger subharmonic humps and higher tonal peaks in the module case. Such subharmonic humps caused by large coherent structures recirculating in the tip gap [13-15] are not seen here.

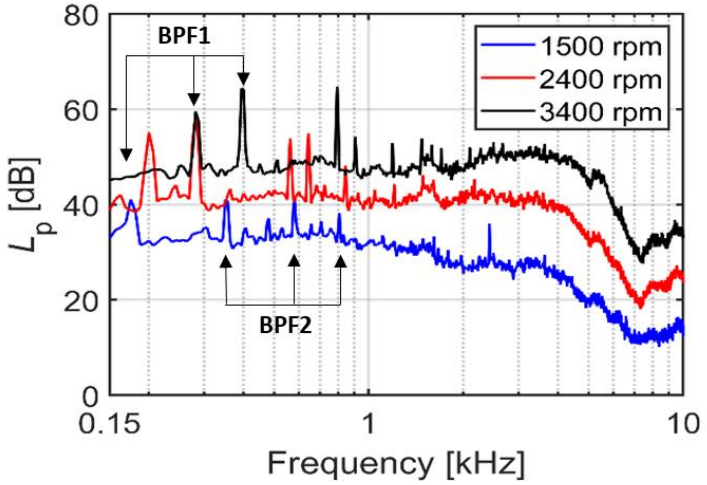

Figure 5: PSD of far-field acoustic pressure on microphone 1 at 3 rotational speeds.

To estimate the nature of the acoustic source in this engine cooling module, the spectra obtained at various rotational speeds on microphone 1 are normalized by different power n of the rotational speed, and presented in Figure 6. Note that the frequency has also been made dimensionless by a Strouhal number, St_t, based on the rotational speed and blade tip chord. Both n = 4 and 5 collapse all spectra in different frequency or Strouhal number range. Similar results are obtained on the other microphones. This thus suggests a dipolar source, which is similar to what was found previously on the smoke-removal fan system [7-8], and is expected given the low Mach number of the fan system. In Figure 6 (left), a good scaling with rpm^5 is observed at Strouhal numbers around 1 (from 0.6 to 2) and stresses that the noise source at the blade tip is chordwise compact at these frequencies. This power 5 is close to the exponent found by Canepa *et al.* [16] for the broadband and tip-leakage noise generated by such automotive engine cooling low-speed fans. Figure 6 (right) shows that the scaling with rpm^4 works well at Strouhal from 2 to 4 at all rotational speeds, except for the lowest speed. This highlights that the noise source becomes chordwise non-compact at high frequencies. The deviation of the case at 1500 rpm may be caused by some significant contribution of the motor. The similar good collapse at lower frequencies is more surprising as this frequency range is strongly affected by vibrations.

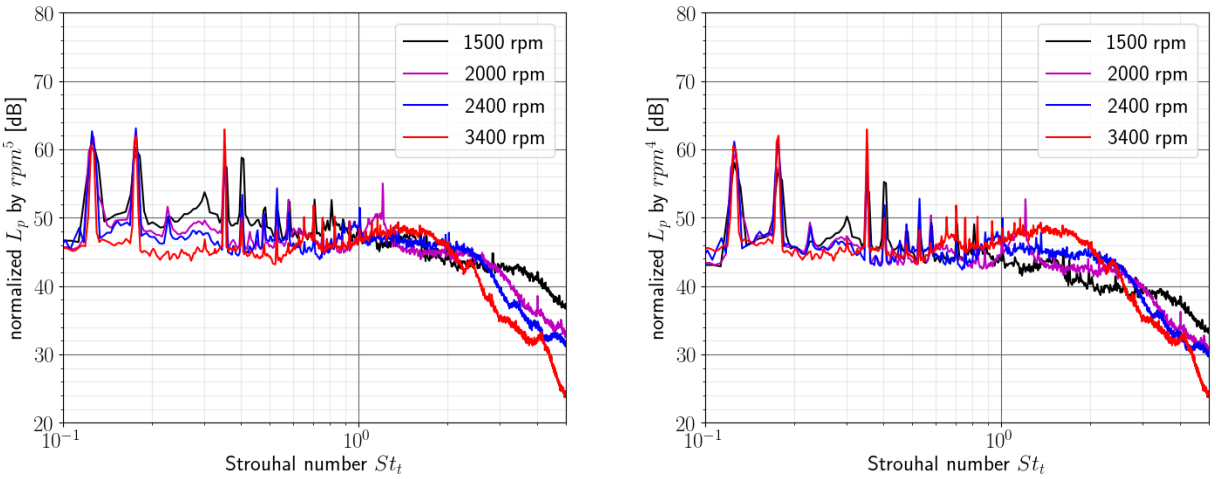

Figure 6: Normalized PSD of far-field acoustic pressure on microphone 1: (left) with rpm^5; (right) with rpm^4.

Noise source localization

To get more precise information about the dipolar noise source evidenced in the previous section and its distribution on the fan, source localization is then performed with the microphone array shown in *Figure 4* and the ROSI algorithm [4]. The algorithm consists of retrieving the acoustic pressure from a moving source measured at each microphone position of the array. The pressure can be calculated using

$$p(\vec{x},t) = \frac{\sigma(\tau_e)}{4\pi\{t-\tau_e+Q(\vec{x},\vec{\xi}(\tau_e),t,\tau_e)\}}$$

in which

$$Q = \left[-\vec{\xi}'(\tau_e) + M\overrightarrow{e_x}\right].\left[\vec{x}-\vec{\xi}(\tau_e) - M(t-\tau_e)\vec{e}_x\right]$$

$\vec{\xi}(t)$ is the moving source and $\vec{x}(t)$ the receiver position. Note that τ_e is the emission time and σ the source strength. The algorithm was implemented in the present paper considering that the rotational speed of the sources is not constant. Several data acquisition have been performed both at UdeS and VKI to check the good repeatability of the measurements.

In Figures 7, 8 and 9, the sound maps are presented in third-octave bands with center frequencies of 4 kHz, 5 kHz, and 6 kHz, for the module configurations with (left) and without (right) heat exchangers. The sources could only be identified above 4 kHz because of the Rayleigh criterion mentioned above. This corresponds to the roll-off portion of the spectrum in *Figure 6.* At lower frequencies, as shown in [6] (Figure 11), the resolution of the antenna is not enough to separate the sources on the fan blades. Indeed, the above Rayleigh criterion applied to a typical distance between two consecutive blades, which can be considered as the minimum separation between two sources, yields a minimum frequency of 3.66 kHz for the present antenna. Yet, in [6], the levels along the fan annulus are already higher along a diagonal direction around 40 degrees following the trigonometric convention. This is confirmed in the present maps (Figures 7, 8 and 9) for both configurations corresponding to two different flow rates for the fan system at the nominal speed of 3400 rpm. The capability to localize sound sources through the heat exchanger is also demonstrated.

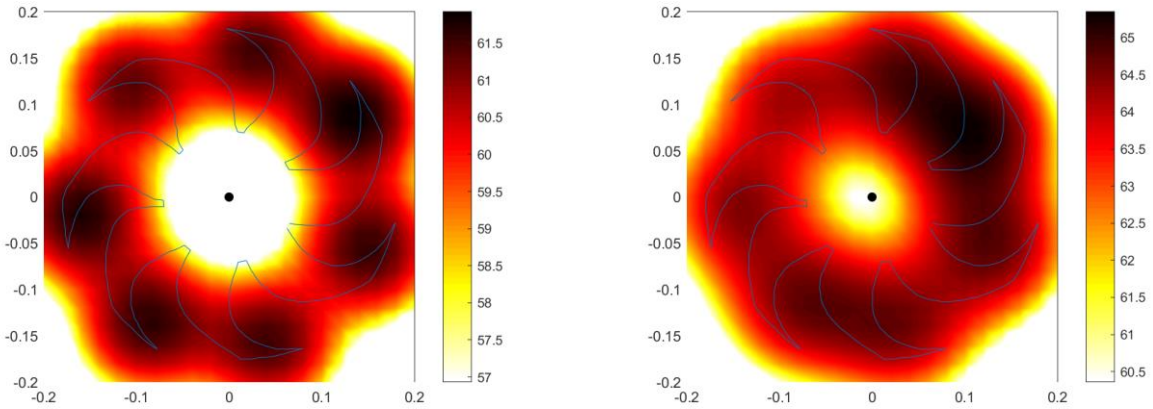

Figure 7: 4 kHz octave band for the module with (left) and without (right) heat exchanger at 3400 rpm.

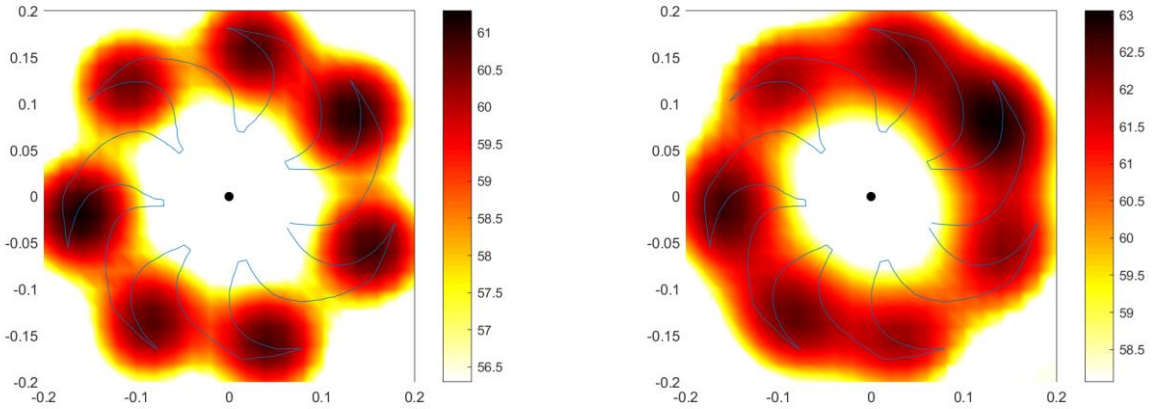

Figure 8: 5 kHz octave band for the module with (left) and without (right) heat exchanger at 3400 rpm.

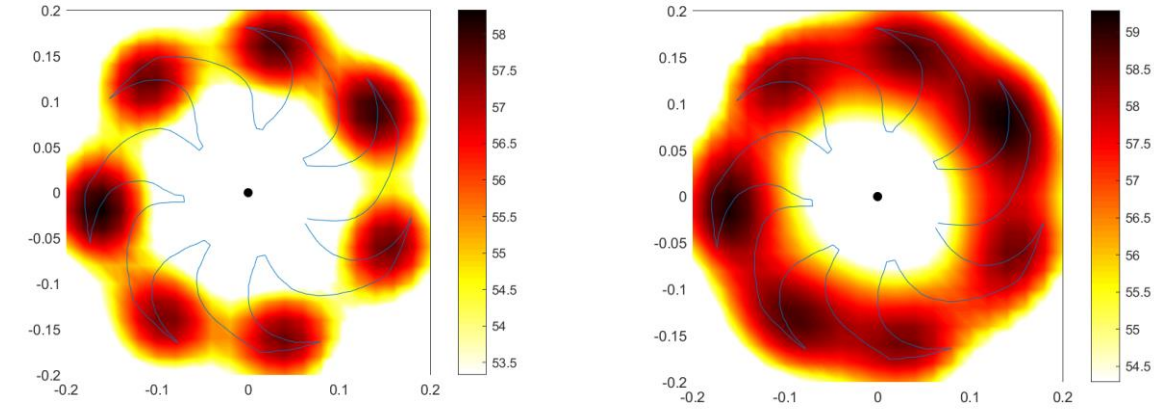

Figure 9: 6.3 kHz octave band for the module with (left) and without (right) heat exchanger at 3400 rpm.

Yet, a difference appears in the radial position of the sources along the blades. Below 4 kHz in [6], the noise source appears more intense at midspan, whereas after the roll-off the noise source moves toward the tip and covers the whole top half of the blade, consistently with the more highly tip-loaded fan (forced vortex). In the tangential direction along the blade chord, the noise source is higher at the leading edge at the tip, most likely caused by the interaction of the tip gap turbulent structures with the fan blades. By comparing the left and right maps in Figures 7, 8 and 9, the same conclusions can be drawn for both flow conditions. Yet, the transition from midspan to tip for the

peak of the noise source seems to occur at higher frequencies without the heat exchanger, and the distribution along the chord seems to be more homogeneous and less concentrated at the leading edge at the transparency flow condition. The importance of the leading-edge tip part of the blade for the present axial fan in terms of noise generation has already been highlighted by Zarri *et al.* [3], especially for frequencies below 3 kHz where the dominant leading-edge noise mechanism has been attributed to the high turbulent-kinetic-energy development in such a loaded blade area.

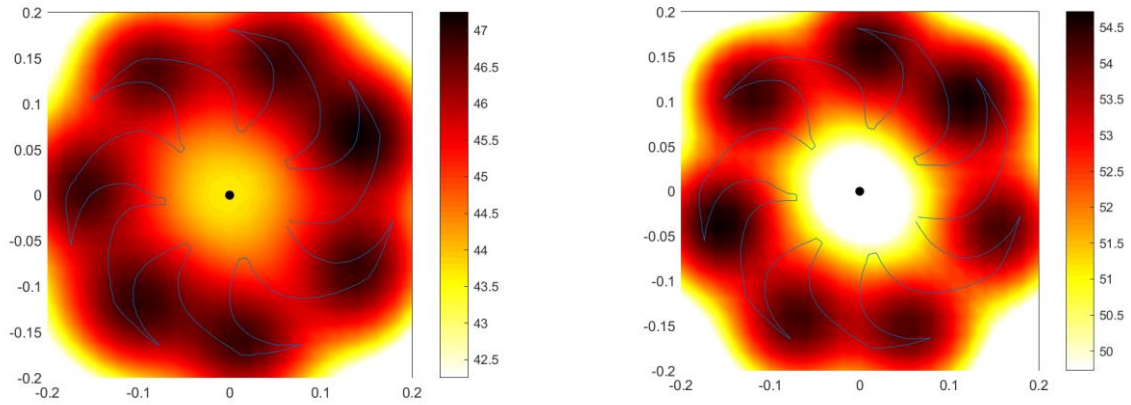

Figure 10: 5 kHz octave band for the full module at 1500 and 2400 rpm

When varying the rotational speed on the module, the flow rate is changed. In *Figure 10*, the radiation maps for the third-octave band centered at 5 kHz are shown for 1500 rpm (left) and 2400 rpm (right) respectively. As expected, the maximum levels of sound decrease with the rotational speed, but the location of the maximum noise sources are still on the top half of the blade, and mostly at the leading edge in the tangential direction. Yet, a larger spanwise portion of the blade is affected by a dynamic range of 4 dB than at 3400 rpm (Figure 8), which is consistent with the corresponding lower flow rate and less adapted flow conditions. This fan seems however quite robust to varying flow conditions without significant change of noise sources.

Finally, the repeatability of the ROSI method as implemented in the present study, has recently been further extended by localizing and quantifying the noise sources on the same module in the VKI ALCOVES anechoic wind tunnel [6]. The sound maps are quasi identical (see Figure 11 and Figure 12 in [6]) and the only differences are caused by the different size and topology of the antenna used in both experiments. Yet, overall excellent agreement is found, which strongly confirms the noise source identification shown above.

CONCLUSION

Noise sources in a typical single-fan automotive engine cooling module have been characterized at several operating conditions obtained by varying both the rotational speed and the volume flow rate. The latter was achieved by removing or not the heat exchanger of the module. This acoustic characterization has combined directivity measurements and microphone-array source localization. The former has allowed some scaling analysis, which has clearly demonstrated the dipolar nature of the sound emitted by the module, and confirmed previous broadband tip noise findings [9-10,16]. The latter has localized the noise sources beyond 4 kHz (the limit of resolution of the current spiral antenna), mostly at the tip blade leading edge for all rotational speeds, with and without the heat exchanger. Therefore, for this particular engine cooling module, the turbulence-interaction noise generated by the secondary flow in the tip region appears to be the broadband noise mechanism that dominates the noise spectra at all the frequencies resolved by ROSI for all the studied flow rates. Finally, the presence of the heat exchanger between the antenna and the fan does not prevent the correct reconstruction of the sound sources obtained with the ROSI technique.

BIBLIOGRAPHY

[1] S. Moreau, "Turbomachinery Noise Predictions: Present and Future," *Acoustics*, **1**: 92–116, 2019.

[2] S. Moreau, "A Review of Turbomachinery Noise: From Analytical Models to High-Fidelity Simulations," in *Fundamentals of High Lift for Future Civil Aircraft*, Editor: Springer Nature Switzerland AG, 2021.

[3] A. Zarri, J. Christophe, S. Moreau and C. Schram, "Influence of Swept Blades on Low-Order Acoustic Prediction for Axial Fans," *Acoustics*, **2**: 812–832, 2020.

[4] P. Sijtsma, S. Oerlemans and H. Holthusen,, "Location of rotating sources by phased array measurements," AIAA 2001-2167 paper, *7th AIAA/CEAS Aeroacoustics Conference (Maastricht, Netherlands)*, 2001.

[5] O. Amoiridis, R. Zamponi, A. Zarri, J. Christophe and C. Schram, "Localization and characterization of rotating noise sources on axial fans by means of an irregularly shaped microphone array," *J. Phys. Conf. Series*, **1909**: 012203:1-9, 2021.

[6] O. Amoiridis, A. Zarri, R. Zamponi, Y. Pasco, G. Yakhina, J. Christophe, S. Moreau and C. Schram, "Sound localization and quantification analysis of an automotive engine cooling module," *J. Sound Vib.*, **517**: 116534:1-18, 2022.

[7] Y. Pasco, S. Moreau, "Acoustic sound radiation of a fire fan system," Fan 2018, International Conference on Fan Noise, Technology and Numerical Methods, Darmstadt, France, April 2018.

[8] Y. Pasco, S. Moreau, "Sound radiation of a smoke-removal fan system," *Acta Acustica united with Acustica Journal*, **105** (1): 86-94, 2019.

[9] M. Piellard, B. Coutty, V. Le Goff, F. Pérot and V. Vidal, "Direct aeroacoustics simulation of automotive cooling fan system: Effect of upstream geometry on broadband noise," AIAA 2014-2455 paper, *20th AIAA/CEAS Aeroacoustics Conference (Atlanta, GA)*, 2014.

[10] D. Lallier-Daniels, M. Sanjosé, S. Moreau and M. Piellard, "Aeroacoustic study of an axial engine cooling module using lattice-Boltzmann simulations and the Ffowcs Williams and Hawkings' analogy," *Eur. J. Mech. B*, **61**: 244-254, 2017.

[11] A. Rynell, G. Efraimsson, M. Chevalier and M. Åbom, "Acoustic characteristics of a heavy-duty vehicle cooling module," *Appl. Acous.*, **111**: 67-76, 2016.

[12] F. Czwielong, F. Kromer and S. Becker, "Experimental investigations of the sound emissions of axial fans under the influence of suction-side exchangers," AIAA 2019-2455 paper, *25th AIAA/CEAS Aeroacoustics Conference (Delft, Netherlands)*, 2019.

[13] S. Magne, S. Moreau and A. Berry, "Subharmonic tonal noise from backflow vortices radiated by low-speed ring rotor in uniform inlet flow," *J. Acous. Soc. America*, **137**(1):198-225, 2015.

[14] S. Moreau and M. Sanjosé, "Sub-harmonic broadband humps and tip noise in low-speed ring fans," *J. Acous. Soc. America*, **139** (1):198-225, 2016.

[15] T. Zhu, D. Lallier-Daniels, M. Sanjosé, S. Moreau and T. Carolus, "Rotating coherent flow structures as a source for narrowband tip clearance noise from axial fans." *J. Sound Vib.* **417**:198-225, 2018.

[16] E. Canepa, A. Cattanei, F.M. Zecchin, G. Milanese and D. Parodi, "An experimental investigation on the tip leakage noise in axial-flow fans with rotating shroud," *J. Sound Vib.* **375**:115–131, 2016.